Spectral characteristics of single and coupled microresonator lasers comprising a replica-molded Bragg grating and dye-doped polymer

J. Zheng,* M. Lu, C. J. Wagner, B. T. Cunningham, and J. G. Eden

Department of Electrical and Computer Engineering, University of Illinois, Urbana, Illinois 61801, USA
**Corresponding author: jzheng5@uiuc.edu*

Received October 11, 2011; accepted October 13, 2011;
posted November 1, 2011 (Doc. ID 154405); published January 13, 2012

Visible microlasers consisting of 80 ± 20 nm thick, dye-doped polymer resonators mated to a second-order, distributed feedback grating having a period of 410 nm exhibit longitudinal mode and spectral characteristics that can be manipulated by microresonator design. Resonators in the form of a square, ring (annulus), or a ring with an intentionally introduced defect ($\pi/2$ section removed) have been examined with respect to the output spectrum, pump energy threshold, and relative slope efficiency of the corresponding microlaser. Although the emission of single rings and arrays of nonoverlapped rings is generally a single mode, the square geometry resonator exhibits a spectrum rich in mode structure, which is attributed partially to degeneracies associated with two coupled Fabry–Perot resonators. Similarly, arrays of coupled (overlapped) rings produce multimode spectra that are skewed toward the blue. For a fixed pump fluence, an array of coupled rings generates output energies at least 50% higher than those for its uncoupled counterpart.

OCIS Codes: 140.3490, 140.2050, 140.3410, 140.7270, 140.3460.

1. INTRODUCTION

Resonator design has assumed a central role in microphotonic devices and systems. Known for their unique optical characteristics with respect to cavity Q and the corresponding reduction in pump energy thresholds for lasing and stimulated nonlinear optical processes, microresonators offer broad functionality as exemplified by the lasers, modulators, and biosensors demonstrated to date [1–4]. The pioneering experiments of Garrett *et al.* [5] on Sm:CaF_2 spheres and Chang and coworkers [6,7] with dye-doped microdroplets identified the whispering gallery modes associated with spherical resonators, and subsequent studies have extended microresonator geometries to include discs, rings, and spiral structures [8–10]. Although the impact of thermal deformation on a spherical microresonator was reported recently [11], less is known of the potential of intentionally introduced defects or coupled arrays of resonators to control the characteristics of microlasers. Several studies have characterized the emission spectra of single microring [12,13] and dye microsphere [14] lasers with respect to resonator diameter and pump intensity. Only recently, however, Zhang *et al.*. [15] employed dye-coated optical fibers to realize as many as four coupled microring lasers.

This article describes the spectral characteristics and threshold behavior of visible microlasers comprising dye-doped polymer microresonators integrated with a distributed feedback grating fabricated by replica molding and operated in second order. Microresonators having the form of a square, a 150 – 600 μm diameter ring, or variants of the ring structure (including coupled and uncoupled arrays), are reported here. The introduction of a defect into a ring, yielding a single ring microresonator in which a $\pi/2$ segment has been removed, has the effect of blueshifting the laser spectrum (relative to that for a single continuous ring) by 1 – 4 nm, producing at least one secondary mode, and increasing the threshold pump energy fluence. Similar behavior is observed when comparing the performance of a single ring with a coupled array in which each ring is in physical contact with one or more of its neighbors. For 532 nm pump fluences below ~1.4 mJ/cm^2, coupled arrays comprising 100 rings (each 150 μm in diameter) generate larger pulse energies per unit active area than do uncoupled arrays in which the ring-to-ring pitch is 10 μm larger than the ring diameter (i.e., rings do not overlap). The results reported here demonstrate the rich microlaser mode structure that is obtainable by manipulating resonator design with coupled arrays or the introduction of specific defects. Such resonators have significant implications for the performance of label-free biosensors based on the shift of laser wavelength or alteration of the laser spectrum by the interaction of an analyte with the resonator.

2. BRAGG GRATING AND MICRORESONATOR FABRICATION

Panel (a) of Fig. 1 is a diagram in cross section of the general laser structure adopted for these experiments. A distributed Bragg grating having a periodicity (Λ) of 410 nm and fabricated by nanoimprint molding provided output coupling for the microresonator. Produced from an Si master fabricated by conventional photolithographic and thin film processing techniques, the grating has a modulation depth of 40 nm and is designed so as to provide extraction (by first-order diffraction) of radiation from the laser cavity at normal incidence to the grating. This second-order distributed feedback (DFB)

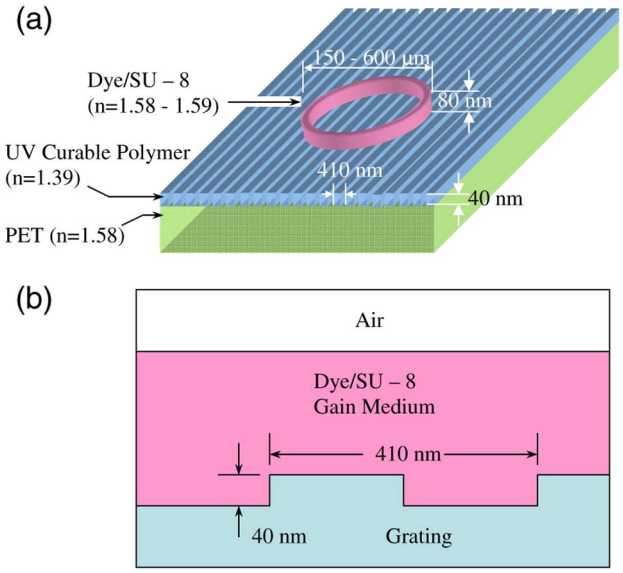

Fig. 1. (Color online) (a) Cross-sectional diagram (not to scale) of the microlaser structure for a single, dye-doped ring microresonator having a mean thickness of 80 nm. The refractive index (n) of each region, as well as several critical dimensions, are indicated. The device is photo-pumped at normal incidence to the plane of the grating by a frequency-doubled Nd: YAG laser. (b) Detailed cross-section of the gain medium/grating structure.

laser is produced on a polyethylene terephthalate (PET) film substrate (having an index of refraction of 1.58) in ultraviolet-curable polymer ($n = 1.39$). Atomic force microscope (AFM) profiles of each grating fabricated in these studies verified that the periodicity was consistently reproducible to within $\pm 1\%$. As an example, Fig. 2 is an AFM profile, highlighting one edge of a dye/SU-8 polymer gain medium layer fabricated on the replica-molded grating. Further details regarding the fabrication of the grating can be found in [16]. The microresonator [shown as a ring in Fig. 1(a)] was fabricated in SU-8 ($n = 1.57$) by doping the polymer host with Rhodamine 6G to an estimated level of 10% by weight and depositing a film of the gain medium onto the grating by a spin-on process, followed by

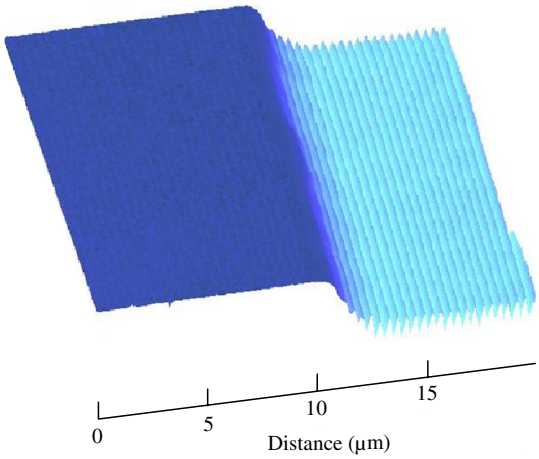

Fig. 2. (Color online) Atomic force microscope (AFM) scan of a portion of a $(425\ \mu m)^2$ dye/SU-8 polymer gain layer fabricated on an underlying replica-molded grating with $\Lambda = 410$ nm.

lithographic patterning to achieve the desired resonator configuration. The lower half of Fig. 1 is an expanded cross-sectional view of a portion of the gain medium/grating structure for which the effective refractive index (n_{eff}) is 1.323.

Several microresonator geometries were investigated in these experiments. Initial studies involved square, dye-doped resonators having an active (surface) area of $425 \times 425\ \mu m^2$ and a mean thickness of 80 ± 20 nm. Repeated observations of microlaser spectra reveal that the peak laser wavelength is insensitive to active layer thicknesses, measured by an AFM and not including the grating modulation depth, in the 60 – 100 nm interval. Subsequent work dealt exclusively with rings (annuli) having diameters of 150 – 600 μm and widths of typically 25 μm. The intent of these studies was to compare the optical characteristics of a single ring oscillator with those of two resonator variants: (1) a "defect ring" comprising a 600 μm diameter ring with a $\pi/2$ section removed, and (2) an array of 100 microrings, each having a diameter of 150 μm and arranged in a 10×10 configuration such that each ring overlaps a portion of at least one of its neighbors. Arrays of uncoupled (nonoverlapped) 300 μm diameter microrings have also been studied.

Experiments involved irradiating a laser chip at normal incidence to the upper surface of the microresonator/gain region with 7 ns FWHM, 532 nm pulses from a frequency-doubled Nd:YAG laser, which provided an energy fluence (E) at the surface of the chip that was continuously adjustable up to ~2 mJ-cm^{-2}. Emission from the optically pumped microchip laser was detected with an optical fiber in tandem with a spectrometer/diode array system having a reciprocal dispersion in first order of 4.1 nm/mm for a 3648 pixel detector array. The fiber has a core diameter of 200 μm, is positioned beneath the chip, and is oriented orthogonal to the PET substrate.

3. EXPERIMENTAL RESULTS

A. Continuous Rings, Uncoupled Ring Arrays

Experiments conducted with microresonators in the form of a single, continuous ring consistently displayed narrow laser emission spectra. Consider, for example, Fig. 3, which compares representative laser spectra for several microchip configurations, each of which is identified in the figure by a simplified (not to scale) diagram of its associated gain medium/resonator geometry. The spectrum of Fig. 3 at far right is that for a 600 μm diameter microring with an annulus width of 25 μm. Having an apparent linewidth of $7 \cdot 10^{-2}$ nm, this laser spectrum is instrument-limited and free of auxiliary mode structure. Of the three individual rings whose output spectra were measured, only one exhibited a weak secondary mode. For this singular spectrum, the observed mode spacing of 0.16 nm is consistent with the expression [12,13]: $\Delta\lambda = \lambda^2(n_{\text{eff}} \cdot 2\pi R)^{-1}$.

Uncoupled arrays of microrings in which the ring pitch (center-to-center spacing) exceeds the microring outer diameter generate emission spectra similar to that for a single ring. An exemplary spectrum is presented in Fig. 3 for a 5×5 array of 300 μm diameter microrings in which the pitch is 310 μm. As one would expect, separating the perimeters of the rings by 10 μm ($\sim 17\lambda$) precludes significant evanescent coupling between any two rings and the array behaves as a collection of isolated rings, producing a single mode output with an instrument-limited linewidth of ≤0.1 nm.

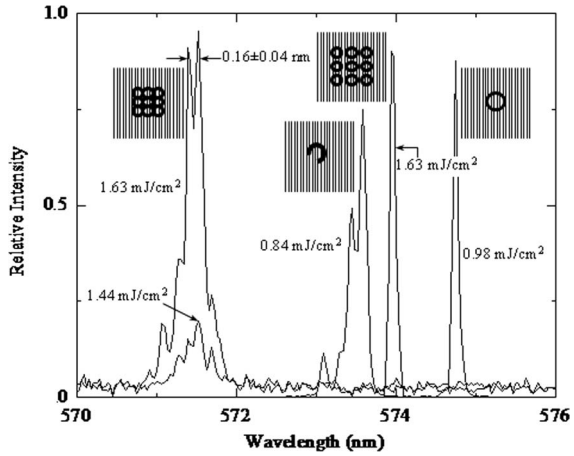

Fig. 3. Comparison of representative laser spectra observed for a dye-doped, continuous ring microresonator, a defect ring, and an array of coupled ring microresonators. For convenience, the spectrum recorded for an array of *uncoupled* (nonoverlapped) ring microresonators is also presented. All of the spectra are identified by diagrams in plan view that are not to scale but qualitatively represent the structure of the associated microlaser. The mean wavelength interval between two local maxima is indicated for the coupled ring spectrum and the pump energy fluence at which each spectrum was recorded is also given.

B. Defect Rings

When a $\pi/2$ segment is removed from a continuous ring resonator, spectra similar to that presented in Fig. 3 are observed. Rather than the single-mode spectrum characteristic of a full ring, significant modal structure is observed and the mean intermode separation is measured to be in the 0.14 – 0.28 nm interval. Defect rings are expected to behave as a Fabry–Perot cavity with a length (for $R = 300$ μm) of ~1400 μm, which corresponds to a mode spacing of 0.09 nm at $\lambda \sim 574$ nm.

An expanded view of the laser spectra produced by two rings and two defect rings, all of which are 600 μm in diameter, is given in Fig. 4. For clarity, the ring spectrum peaking at ~575.44 nm has been downshifted by 1.0 nm so as not to overlap the other continuous ring profiles. Also, each spectrum is shown for two values of the pump energy density, both of which are ≤1.1 mJ-cm^{-2}. All three of the defect rings examined in these experiments exhibited at least one strong secondary mode, whereas only one of the three continuous rings produced an auxiliary mode. In the latter case, the secondary mode weakened rapidly (relative to the stronger peak) with increasing pump intensity. Note also in Figs. 3 and 4 that, despite chip-to-chip variations in the peak lasing wavelength of no more than ±0.7 nm, the defect ring spectra consistently lie to the blue of their full ring counterparts. It is also clear from Figs. 3 and 4 that the mode splitting observed for the defect rings is larger (by almost a factor of 1.7) than that for the one continuous ring spectrum having a secondary peak.

Pauzauskie *et al.* [13] have discussed in detail several distinctions between a full (continuous) ring and an open resonator, and the reproducible blueshift of the defect ring spectra (Figs. 3 and 4) with respect to the single ring emission is consistent with similar observations of nanowire ring resonators. In effect, breaking the ring increases the threshold gain and shifts the laser spectrum to higher photon energies. Furthermore, the introduction of the $\pi/2$ defect adversely impacts the laser threshold pump energy. For a continuous ring, the threshold pump energy density is measured to be ~0.38 mJ-cm^{-2}, or ~10% lower than that recorded for the defect ring (≥0.42 mJ-cm^{-2}). Although the difference between the threshold pump energies of the two rings is statistically significant, the magnitude of the difference is less than anticipated. Somewhat surprisingly, the resonators exhibit slope efficiencies that are approximately equal.

The integration of the $\Lambda = 410$ nm grating with the gain medium in these experiments profoundly impacts both laser threshold and mode structure. Since the periodicity of the DFB grating is roughly 3 orders of magnitude smaller than the surface dimensions of the microresonators, only those modes supported by both the grating and the microresonator will be amplified. This consideration and the characteristics of the Bragg grating formed in a curable polymer ($n = 1.39$) are responsible for the spectra of Figs. 3 and 4 lying in the 571 – 577 nm region despite the fact that peak emission for the dye/polymer gain medium occurs at ~582 nm (FWHM of ~13 nm). As a consequence, few optical modes are observed to lase, and the resonators cannot be viewed as optically isolated from the grating.

C. Arrays of Coupled Rings

For a coupled ring array, every metric of performance—spectrum, output energy, and efficiency—differs significantly from those for the uncoupled version or a single ring. The spectrum presented in Fig. 3 is that for an array of 100 microresonators coupled by patterning 150 μm diameter rings with a pitch of ~125 μm so as to ensure that each ring is in physical contact with at least one of its nearest neighbors. Indeed, this value of pitch ensures that each ring fully overlaps a section of all contiguous rings. The diameter of the rings in this coupled array was chosen so as to nearly equalize the surface area (and volume) of the dye-doped polymer regions of both the uncoupled and coupled arrays. For the 5×5 arrays of 300 μm diameter, nonoverlapping (uncoupled) rings, the dye-doped (gain region) surface area is 0.54 cm^2, while that for the 10×10 array of coupled, 150 μm diameter rings was measured to

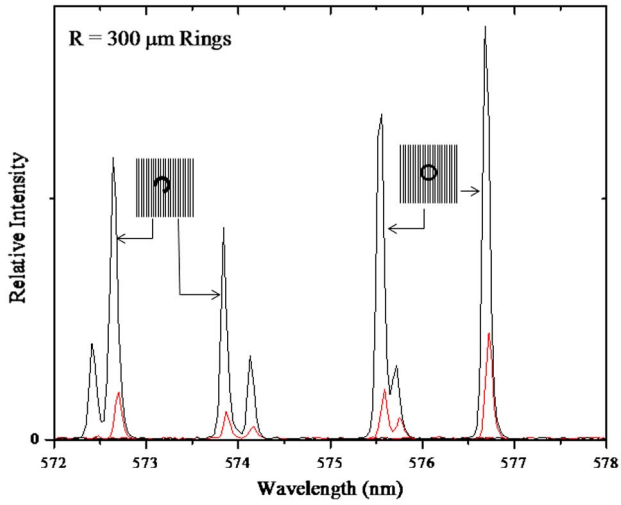

Fig. 4. (Color online) Expanded view of the photo-pumped laser spectra for two ring and two defect ring microresonators, all having a radius (R) of 300 μm. The width of each annulus is 25 μm. The only continuous ring spectrum exhibiting a secondary mode is shown but, for the sake of clarity, this spectrum has been shifted to shorter wavelengths by ~1.0 nm. Data are shown for two values of pump intensity, both of which are ≤1 mJ-cm^{-2}.

be 0.73 cm^2. Thus, the gain region surface areas for the two arrays differ by a factor of 1.35.

It is evident in Fig. 3 that the spectrum for the coupled array is blueshifted from the uncoupled array emission peak at ~574.0 nm by ~2.5 nm. Furthermore, the coupled array introduces as many as six detectable secondary longitudinal modes having an average spacing of $\Delta\lambda = 0.16$ nm, which is consistent with the circumference for a single, 150 μm diameter ring. However, this value of intermodal separation is approximately one-half of that calculated from the expression cited earlier ($\Delta\lambda = \lambda^2(n_{\text{eff}} \cdot 2\pi R)^{-1} \approx 0.29$ nm), and COMSOL simulations of the mode structure in smaller rings predict that mode spacings, which are as large as 0.12 nm for 2–4 coupled ring resonators and $R = 300$ μm, depend strongly on the position at which the resonator is excited. It should also be noted that pulling of each mode to the blue is evident as the pump energy fluence is increased. This is particularly noticeable for the emission peak that, for a single pulse pump fluence of 1.5 mJ-cm^{-2}, lies at ~571.52 nm.

Extensive measurements of the output pulse energy generated by the 10×10 coupled array, relative to that for the 5×5 uncoupled configuration, demonstrate that the coupled array is the more efficient of the two. For $E \leq 1.4$ mJ-cm^{-2}, the coupled array is found to have an optical-to-optical conversion efficiency more than three times larger than that for the uncoupled array of resonators. After normalizing the results to the relative active areas of the two arrays (which differ by ~35%), the coupled array continues to be considerably more efficient. This conclusion is less valid at higher pumping fluences, where the improvement in the efficiency of the coupled array, relative to that for the uncoupled version, falls slightly but the difference remains. Furthermore, for a fixed value of the pump laser fluence, the array of coupled rings generates output energies at least 50% higher than those for its uncoupled counterpart.

D. Square Resonators

Despite considerable care given to strictly controlling the composition and dimensions of the gain region in all of the lasers investigated in these experiments, variations in both the peak wavelength of the laser emission and the mode structure were observed (as noted previously). In order to assess the magnitude of the fluctuations in spectral profile and laser wavelengths that could be expected from a larger sample set, a series of 15 microlaser chips, each having a square active region with an area of (425 μm)^2, was fabricated and tested. Measurements found that the peak laser wavelength varied from 570.8 nm to 579.4 nm but the distribution of wavelengths for the set was well-described by a Gaussian having a central wavelength of 575.5 nm and an FWHM of 1.7 nm. Fluctuations in the emission profiles from chip-to-chip were also observed but virtually all displayed considerable mode structure, as illustrated by the representative laser spectra of Fig. 5 for two separate chips. Data are presented for pump energy fluences of 0.54 mJ-cm^{-2} (solid circles: •) and 0.74 mJ-cm^{-2} (open circles: ∘). Each of the spectra shown in the figure exhibit maximum emission in the 575 – 576.5 nm region and periodic structure extending toward the blue. More than 65 measurements of the spectral interval ($\Delta\lambda$) between adjacent secondary emission peaks, for all of the square microresonator lasers studied, yielded $\Delta\lambda = 0.17 \pm 0.09$ nm (where the uncertainty represents 1 standard deviation in the measurements), a value which is within 1σ of the longitudinal mode spacing ($\Delta\lambda \approx 0.24$ nm) expected for a resonator 425 μm in length and encompassing a medium with $n = 1.58$. The discrepancy between the calculated and observed values is attributed to a nonuniform refractive index, variations in thickness of the gain medium (owing to variations in the polymer/dye mixture), and slight dimensional errors. Measurements of the dependence of the relative output energy on the pump energy fluence are summarized in Fig. 6 for the 425 μm square resonator lasers. The error bars in the figure represent the estimated uncertainty in each measurement. The threshold pump fluence is measured to be ~0.25 mJ-cm^2 and a least-squares fit of a polynomial to the $E \geq 0.36$ mJ-cm^{-2} data (illustrated by the solid curve of Fig. 3) demonstrates that the variation of the laser output power with increasing pump energy is nearly quadratic, a functional dependence that often arises from reabsorption in the gain medium.

E. Biosensor Applications

Optical biosensors have typically detected the presence and nature of an analyte by monitoring the shift in the wavelength of a laser, a coupling angle, or the strength of an optical

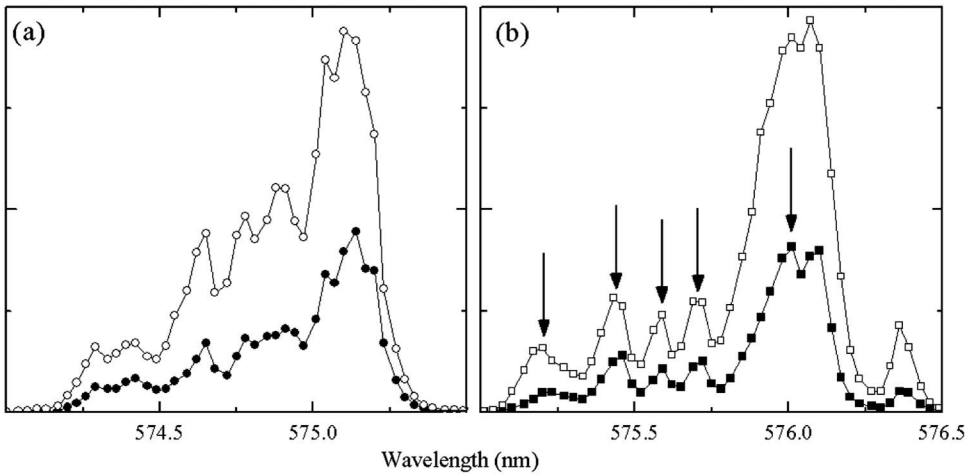

Fig. 5. Emission spectra for two microlasers, each having a square microresonator with an active area of (425 μm)^2. Solid circles (•) denote spectra recorded for a pump energy fluence of 0.54(±0.04) mJ-cm^{-2} and the open circles (∘) represent data acquired at 0.74(±0.04) mJ-cm^{-2}. Several reproducible, secondary peaks are identified in panel (b) by vertical arrows.

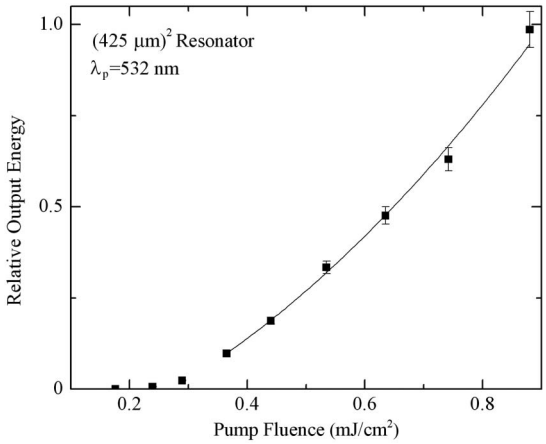

Fig. 6. Dependence of the relative laser output pulse energy on the 532 nm laser energy fluence for a 425 μm square microresonator. Error bars represent the estimated uncertainty for each measurement and the solid curve is a least-squares fit of a polynomial to the data.

resonance [4]. Each of these faces fundamental restrictions with respect to sensitivity and, in this regard, several general observations concerning the utility of the microlaser structures reported here for biosensor applications are warranted. The first is that experiments and simulations show the laser spectra for the structures of Fig. 1 to be determined by the combined effect of the microresonator and the grating. For example, comparisons of the spectra produced by the square microresonator/grating structures (Fig. 5) with those produced by the grating alone (uniformly dye-doped) were made at a pump fluence of ~0.9 mJ-cm^{-2}. The grating itself produced a single narrow line peaking at ~602.3 nm, which contrasts starkly with the multimode, blueshifted spectra of Fig. 5. One concludes that the square resonators, acting in concert with the Bragg grating, shift the center wavelength of the laser spectrum but, perhaps more importantly, alter the mode structure dramatically.

Secondly, the specific profile for the laser spectrum emitted by a given resonator/grating design is sensitive to slight variations ($< \pm$ 10 nm) in the thickness of the active region and the topology of the resonator. For example, changes of several

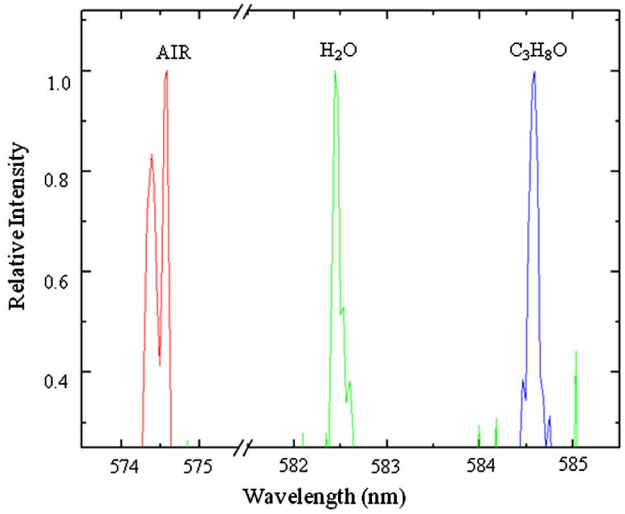

Fig. 7. (Color online) Normalized laser spectra for a (425 μm)^2 square microresonator in contact with air (red curve), deionized water (green), and isopropyl alcohol (C_3H_8O, blue).

nanometers in the depth of the square resonator (Fig. 5) resulted in the rapid growth of the longest wavelength mode (relative to the primary peaks) and the suppression of the weaker modes to the blue. Such clear distinctions in the spectra of microlasers, fabricated in the same processing batch but having small differences in dimensions, suggest that the resonant mode(s) associated with a resonator integrated with the one-dimensional photonic crystal will be unusually sensitive to modifications of either the surface environment or bulk properties of the laser structure. Such a degree of sensitivity would represent a decided asset for label-free biosensing.

To that end, Fig. 7 presents three normalized laser spectra for a single microlaser chip having the square resonator of Fig. 5. With the pumping fluence held constant (at ≤1 mJ-cm^{-2}), the spectrum of the laser was recorded when the microresonator was in contact with air, water, or isopropyl alcohol (C_3H_8O). It is clear from Fig. 7 that the medium external to the microresonator alters not only the peak wavelength but the mode structure as well. This behavior has several implications for biosensors, one of which is that the detection floor can now be lowered because an analyte shifts the laser spectrum but also transforms its profile. Previous sensors have relied almost exclusively on the former of these but detecting only the wavelength shift arising from the interaction of a gain medium with an analyte severely restricts the sensitivity of the sensor.

4. SUMMARY AND CONCLUSIONS

Optically pumped plastic microlasers having a patterned, dye-impregnated polymer gain region in contact with a Bragg grating have been investigated with resonators in the form of a ring, a ring with a $\pi/2$ segment removed, and a square. Arrays of uncoupled rings produce spectra virtually indistinguishable from that for a single ring. Owing to the exponential decay of evanescent field strengths with distance from the ring perimeter, optical coupling between rings in an array is expected to be negligible unless the ring perimeters are separated by no more than 1–2 wavelengths. In contrast, arrays of coupled (overlapped) rings exhibit laser pump energy thresholds significantly lower than those measured for its uncoupled counterpart. The introduction of a $\pi/2$ defect into a ring has the effect of blueshifting the laser spectrum while simultaneously generating one or more weaker, secondary modes. Similarly, square microresonators generate laser spectra characterized by as many as six secondary peaks associated with longitudinal modes of the resonator. The spectra reported here have significant implications for the design and performance of label-free biosensors [4] in that the multiple mode structure of several resonator geometries can be viewed as a tool augmenting the precise measurement of small shifts in the laser emission wavelength resulting from perturbation of the evanescent resonator field by an analyte. Preliminary experiments conducted with a liquid in contact with a microlaser demonstrate both laser wavelength shifts and the transformation of the laser spectral profile that will facilitate the automated detection of a specific biological molecule or cell.

ACKNOWLEDGMENTS

The expert technical assistance of V. Mowery and C. Coxsey, as well as the support of this work by the U. S. Air Force Office of Scientific Research under grant FA9550-07-1-0003, are gratefully acknowledged.

REFERENCES

1. R. Chang and A. J. Campillo, eds., *Optical Processes in Microcavities* (World Scientific, 1996).
2. W. von Klitzing, E. Jahier, R. Long, F. Lissillour, V. Lefévre-Seguin, J. Hare, J.-M. Raimond, and S. Haroche, "Very low threshold green lasing in microspheres by up-conversion of IR photons," J. Opt. B **2**, 204–206 (2000).
3. L. Zhang, M. Song, T. Wu, L. Zou, R. G. Beausoleil, and A. E. Willner, "Embedded ring resonators for microphotonic applications," Opt. Lett. **33**, 1978–1980 (2008).
4. M. Lu, S. S. Choi, C. J. Wagner, J. G. Eden, and B. T. Cunningham, "Label free biosensor incorporating a replica-molded, vertically emitting distributed feedback laser," Appl. Phys. Lett. **92**, 261502 (2008).
5. C. G. B. Garrett, W. Kaiser, and W. L. Bond, "Stimulated emission into optical whispering modes of spheres," Phys. Rev. **124**, 1807–1809 (1961).
6. H.-M. Tzeng, K. F. Wall, M. B. Long, and R. K. Chang, "Laser emission from individual droplets at wavelengths corresponding to morphology-dependent resonances," Opt. Lett. **9**, 499–501 (1984).
7. S.-X. Qian, J. B. Snow, H.-M. Tzeng, and R. K. Chang, "Lasing droplets: highlighting the liquid-air interface by laser emission," Science **231**, 486–488 (1986).
8. S. L. McCall, A. F. J. Levi, R. E. Slusher, S. J. Pearton, and R. A. Logan, "Whispering-gallery mode microdisk lasers," Appl. Phys. Lett. **60**, 289–291 (1992).
9. L. Yang, D. K. Armani, and K. J. Vahala, "Fiber-coupled erbium microlasers on a chip," Appl. Phys. Lett. **83**, 825–826 (2003).
10. M. Hentschel and T.-Y. Kwon, "Designing and understanding directional emission from spiral microlasers," Opt. Lett. **34**, 163–165 (2009).
11. Y.-F. Xiao, C.-H. Dong, C.-L. Zou, Z.-F. Han, L. Yang, and G.-C. Guo, "Low-threshold microlaser in a high-Q asymmetrical microcavity," Opt. Lett. **34**, 509–511 (2009).
12. S. V. Frolov, Z. V. Vardeny, and K. Yoshino, "Plastic microring lasers on fibers and wires," Appl. Phys. Lett. **72**, 1802–1804 (1998).
13. P. J. Pauzauskie, D. J. Sirbuly, and P. Yang, "Semiconductor nanowire ring resonator laser," Phys. Rev. Lett. **96**, 143903 (2006).
14. H. Li, L. Lei, Q. Zeng, J. Shi, C. X. Luo, H. Ji, Q. Ouyang, and Y. Chen, "Laser emission from dye doped microspheres produced on a chip," Sens. Actuators B Chem. **145**, 570–574 (2010).
15. X. Zhang, H. Li, X. Tu, X. Wu, L. Liu, and L. Xu, "Suppression and hopping of whispering gallery modes in multiple-ring-coupled microcavity lasers," J. Opt. Soc. Am. B **28**, 483–488 (2011).
16. M. Lu, S.-J. Park, B. T. Cunningham, and J. G. Eden, "Vertically emitting, dye-doped polymer laser in the green ($\lambda \sim 536$ nm) with a second order distributed feedback grating fabricated by replica molding," Opt. Commun. **281**, 3159–3162 (2008).